SCIENCE CHINA
Physics, Mechanics & Astronomy

• Article •

January 2015 Vol. 58 No. 1: 014501
doi: 10.1007/s11433-014-5567-1

Solar sailing trajectory optimization with planetary gravity assist

CAI XingShan, LI JunFeng & GONG ShengPing*

School of Aerospace, Tsinghua University, Beijing 100084, China

Received January 10, 2014; accepted June 13, 2014; published online September 28, 2014

Significant propellant mass saving can be obtained with the use of complex multiple intermediate flyby maneuvers for conventional propulsion systems, and trip time also decreases for a portion of the proper solar sail missions. This paper discusses the performance of gravity assist (GA) in the time-optimal control problem of solar sailing with respect to sail lightness number and the energy difference between the initial and final orbit in the rendezvous problem in a two-body model, in which the GA is modeled as a substantial change in the velocity of the sailcraft at the GA time. In addition, this paper presents a method to solve the time-optimal problem of solar sailing with GA in a full ephemeris model, which introduces the third body's gravity in a dynamic equation. This study builds a set of inner constraints that can describe the GA process accurately. Finally, this study presents an example for evaluating the accuracy and rationality of the two-body model's simplification of GA by comparison with the full ephemeris model.

solar sailing trajectory optimization, gravity assist, full ephemeris model

PACS number(s): 96.12.De, 02.30.Yy, 95.55.Pe

Citation: Cai X S, Li J F, Gong S P. Solar sailing trajectory optimization with planetary gravity assist. Sci China-Phys Mech Astron, 2015, 58: 014501, doi: 10.1007/s11433-014-5567-1

1 Introduction

The solar sail has been considered to be one of the most promising propulsion systems without fuel consumption [1,2]. In contrast to conventional propulsion systems for spacecraft, solar sails are continuously accelerated to escape the solar system [3] or spiral inward to the inner solar system [4]. With the second booming of deep space exploration, the solar sail has attracted increasing levels of attention. In 2010, Japan's IKAROS [5] spacecraft became the first vehicle successfully accelerated only by solar radiation pressure, which enhanced confidence in solar sail development. Because solar sailing has great advantages in interplanetary missions [6,7], it has been investigated in various areas, such as attitude control [8], passive stability design [9–11], trajectory optimization [12–14] and mission analysis [15].

Large energy transformations of spacecraft need to be completed when the target is far from the initial orbit, and gravity assist (GA) has been introduced to lower the energy increment. Such an approach has been adopted in the MESSENGER mission, of which the spacecraft trajectory used one Earth flyby, two Venus flybys, and three Mercury flybys during its flight toward the closest planet to the Sun [16]. However, although the use of multiple flyby maneuvers substantially reduces the total mission energy increment, it increases both the mission complexity and the trip time. For time optimal problem of the solar sail, GA may play an undesirable role in reducing the trip time. Quarta and Mengali investigated the solar sail missions to Mercury with a single Venus GA [17] and analyzed the effect of GA in the solar sail problem using a polar inertial frame in the coplanar condition.

Most studies involve multiple flyby interplanetary trajectories in a two-body model, in which the spacecraft is subject only to the gravitational force of the center of mass

*Corresponding author (email: gongsp@tsinghua.edu.cn)

and the spacecraft's own solar radiation pressure. Broucke [18] used linked conics in a two-body model and introduce the flyby maneuver to increase or decrease the orbit energy. Prado [19] measured the GA time via a combination of the impulsive maneuvers and GA. Felipe et al. [20,21] sorted the trajectory by analyzing the mechanical energy of the spacecraft and the GA planet. All of the abovementioned research treated the GA in the linked-conics model (two-body model), in which the GA planet was considered massless, and the GA was modeled as an instantaneous velocity increment. There is rare literature studying GA in a full ephemeris model. Bayliss [22] researched GA by considering the third body's gravity perturbation in a two-body model, which did not avoid linking the trajectory, and the procedure was highly complicated. Cai et al. [23] considered the GA in low-thrust trajectory optimization in a full ephemeris model.

The reasons outlined above demonstrate that the employment of GA should be carefully investigated when GA can decrease the trip time in the time optimal problem of solar sails. Literature on solar sails with GA is rare. The first part of this paper quantifies the improvement (in terms of mission time saving) that a single GA offers with respect to a classical direct transfer (DT) and analyzes the changing of trip time relative to the sail lightness number and the energy difference between the initial and final orbit numerically.

For a practical mission, the spacecraft is subject to a third body's gravity, especially the GA planet's gravity, and the "zero-sphere-of-influence patched conic" cannot describe the real GA process. The second part of this paper presents a method to solve an accurate many-body reference trajectory in a full ephemeris model that introduces the third body's gravity in dynamic equations. At the same time, to describe the GA process, this study builds a set of 3-D equivalent inner equality constraints, which constrains the actual orbit inclination, the perigee distance and the true anomaly relative to the GA planet. This paper uses an indirect method to solve the problem [24,25].

2 Gravity assist in a two-body model

2.1 The mathematical model

In a two-body model, the dynamic equation for a perfectly reflecting solar sail in a Sun-centered orbit is written as:

$$\dot{\boldsymbol{r}} = \boldsymbol{v}, \dot{\boldsymbol{v}} = -\frac{\mu}{r^3}\boldsymbol{r} + \frac{\beta\mu(\boldsymbol{r}\cdot\boldsymbol{n})^2}{r^4}\boldsymbol{n}, \tag{1}$$

where $\boldsymbol{r}$ and $\boldsymbol{v}$ denote the position and velocity of the sailcraft in the heliocentric ecliptic reference system (HECS), respectively. The sun's gravitational constant is denoted by μ, $1.32712440018\times10^{11}\,\mathrm{km^3/s^2}$. β is the sail lightness number.

Figure 1 shows the sail sailing altitude control angles in the orbital coordinate system, where *s-rth* is a Heliocentric orbital coordinate system. The origin of coordinates *s* is at the solar sailing's center of mass, *sr* axis is in the same direction of incident sunlight, *sh* axis is along the direction of normal vextor of solar sailing's orbit, *st* axis, *sr* axis and *sh* axis constitute a right-handed coordinate system. The control variable is the normal vector of the solar sail $\boldsymbol{n}$, which has the form of

$$\boldsymbol{n} = (\cos\alpha, \sin\alpha\cos\delta, \sin\alpha\sin\delta)^{\mathrm{T}}, \alpha \in \left[0, \frac{\pi}{2}\right], \delta \in [0, 2\pi), \tag{2}$$

where α and δ denote the cone angle and clock angle described by Figure 1, and they consist of the control vector $\boldsymbol{u}(\alpha, \delta)$.

The minimum time trajectory is obtained with the aid of an indirect approach, from Pontryagin's maximum principle (PMP), requires the maximization of the following Hamiltonian function $\boldsymbol{H}$:

$$H = \boldsymbol{\lambda}_r \cdot \boldsymbol{v} + \boldsymbol{\lambda}_v \cdot \left(-\frac{\mu}{r^3}\boldsymbol{r} + \frac{\beta\mu(\boldsymbol{r}\cdot\boldsymbol{n})^2}{r^4}\boldsymbol{n}\right) - 1, \tag{3}$$

where $\boldsymbol{\lambda}_r$ and $\boldsymbol{\lambda}_v$ are the functional Lagrange multipliers whose time derivative is given by the following equations:

$$\dot{\boldsymbol{\lambda}}_r = \frac{\mu}{r^3}\boldsymbol{\lambda}_v - \frac{3\mu\boldsymbol{r}\cdot\boldsymbol{\lambda}_v}{r^5}\boldsymbol{r} - 2\beta\mu(\boldsymbol{r}\cdot\boldsymbol{n})(\boldsymbol{\lambda}_v\cdot\boldsymbol{n}) \times\left(\frac{1}{r^4}\boldsymbol{n} - \frac{2(\boldsymbol{r}\cdot\boldsymbol{n})}{r^6}\boldsymbol{r}\right), \dot{\boldsymbol{\lambda}}_v = -\boldsymbol{\lambda}_r. \tag{4}$$

The optimal normal vectors of a solar sail, which are the maximum of the Hamiltonian, are determined by [14]

$$\boldsymbol{n} = \cos\alpha\frac{\boldsymbol{r}}{r} + \sin\alpha\boldsymbol{w}, \tag{5}$$

where

$$\alpha = \begin{cases} \tan^{-1}\dfrac{-3+\sqrt{9+8\tan^2\tilde{\alpha}}}{4\tan\tilde{\alpha}}, & \tilde{\alpha} \leqslant 90°, \\ \tan^{-1}\dfrac{-3-\sqrt{9+8\tan^2\tilde{\alpha}}}{4\tan\tilde{\alpha}}, & \tilde{\alpha} > 90°, \end{cases} \tag{6}$$

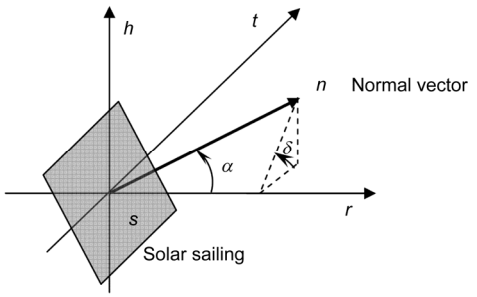

Figure 1 Sail sailing altitude control angles in the orbital coordinate system.

and

$$\frac{\boldsymbol{\lambda}_v}{\lambda_v} = \cos\tilde{\alpha}\frac{\boldsymbol{r}}{r} + \sin\tilde{\alpha}\boldsymbol{w},$$

where $\boldsymbol{w}$ denotes the unit vector, which is perpendicular to $\boldsymbol{r}$ and lies on the plane defined by $\boldsymbol{r}$ and $\boldsymbol{\lambda}_v$, and $\tilde{\alpha}$ denotes the angle between $\boldsymbol{r}$ and $\boldsymbol{\lambda}_v$.

Eqs. (1) and (4) represent a system of twelve first-order differential equations. By taking into account the functional dependence given by eqs. (5) and (6), they can be rewritten in the compact form as:

$$\dot{\boldsymbol{x}} = \boldsymbol{f}(\boldsymbol{x}) \quad \text{with} \quad \boldsymbol{x} \triangleq \left[\boldsymbol{r}, \boldsymbol{v}, \boldsymbol{\lambda}_r, \boldsymbol{\lambda}_v\right]^{\mathrm{T}}. \tag{7}$$

The optimal trajectory can be obtained by numerically integrating eq. (7) in the time interval $t \in [t_0, t_f]$ because the twelve suitable boundary conditions are given.

2.2 Constraints

Let us consider the simplest rendezvous problem, in which the sailcraft starts from the asteroid 1 and targets the asteroid 2 with a single planet GA during the mission.

2.2.1 Sailcraft launch ($t=t_0$)

At the initial time t_0, the sailcraft has the same position and velocity of asteroid 1:

$$\boldsymbol{r}\left(t_0\right) - \boldsymbol{r}_{As1}\left(t_0\right) = 0,\ \boldsymbol{v}\left(t_0\right) - \boldsymbol{v}_{As1}\left(t_0\right) = 0, \tag{8}$$

which corresponds to the Lagrange numerical multipliers $\boldsymbol{\chi}_{1\sim6}$. $\boldsymbol{r}_{As1}(t_0)$ and $\boldsymbol{v}_{As1}(t_0)$ denote the position and velocity of Asteroid 1 at time t_0 in HECS.

2.2.2 Midcourse flyby ($t=t_m$)

In the two-body model, the GA is modeled such that the sailcraft velocity suffers a sudden change, namely, the direction of hyperbolic excess velocity $\boldsymbol{v}_\infty$ obtains a substantial change of angle θ, due to the GA effect [18].

The time spent inside planetary influence is neglected. The sailcraft positions just before and after GA are both required to be equal to the GA planet position. The magnitude of hyperbolic excess velocity remains invariant immediately before and after GA. The rotation angle θ that $\boldsymbol{v}_\infty$ is turned during the GA depends on the periapsis radius r_{p} of the sailcraft relative to the GA planet and the magnitude of the hyperbolic excess velocity $\boldsymbol{v}_\infty$. These relationships, which correspond to Lagrange numerical multipliers $\boldsymbol{\chi}_{\mathrm{GA1\text{-}4}}^{\mathrm{TBM}}$, $\kappa_{\mathrm{GA}}^{\mathrm{TBM}}$, are expressed by

$$\boldsymbol{\psi}_{\mathrm{GA}}^{\mathrm{TBM}} \triangleq \begin{pmatrix} \boldsymbol{r}\left(t_m\right) - \boldsymbol{r}_a\left(t_m\right) \\ v_\infty^- - v_\infty^+ \end{pmatrix} = \boldsymbol{0}, \tag{9}$$

$$\sigma_{\mathrm{GA}}^{\mathrm{TBM}} \triangleq -1 + r_{\mathrm{p}} / r_{\min} \geqslant 0, \tag{10}$$

where

$$r_p = \frac{\mu_a}{v_\infty^- v_\infty^+}\left(\frac{1}{\sin\theta/2} - 1\right),$$

$$\cos\theta = \boldsymbol{v}_\infty^- \cdot \boldsymbol{v}_\infty^+ / v_\infty^2,$$

where the superscript TBM denotes the quantities in the two-body model, superscripts – and + denote the quantities, respectively, just before and after GA, t_m is the date on which GA occurs, μ_a denotes the gravitational constant of the GA planet and $r_{\min}$ is the minimal admissible periapsis radius.

2.2.3 Rendezvous ($t=t_f$)

At the final instant, when the sailcraft has reached the targeting orbit, it has the same position and velocity of asteroid 2:

$$\boldsymbol{r}\left(t_f\right) - \boldsymbol{r}_{As2}\left(t_f\right) = 0,\ \boldsymbol{v}\left(t_f\right) - \boldsymbol{v}_{As2}\left(t_f\right) = 0, \tag{11}$$

which corresponds to the Lagrange numerical multipliers $\boldsymbol{\chi}_{7\sim12}$. $\boldsymbol{r}_{As2}(t_f)$ and $\boldsymbol{v}_{As2}(t_f)$ denote the position and velocity of Asteroid 2 at time t_f in HECS.

2.3 Nonlinear equation solver

According to the PMP, the boundary transversal conditions are

$$\begin{cases} \boldsymbol{\lambda}_r\left(t_0\right) + \boldsymbol{\chi}_{1\text{-}3} = 0, \\ \boldsymbol{\lambda}_v\left(t_0\right) + \boldsymbol{\chi}_{4\text{-}6} = 0, \\ -\boldsymbol{\lambda}_r\left(t_f\right) + \boldsymbol{\chi}_{7\text{-}9} = 0, \\ -\boldsymbol{\lambda}_v\left(t_f\right) + \boldsymbol{\chi}_{10\text{-}12} = 0, \end{cases} \tag{12}$$

and the boundary stationary conditions are

$$-H\left(t_0\right) - \boldsymbol{\chi}_{1\text{-}3} \cdot \boldsymbol{v}_{As1}\left(t_0\right) - \boldsymbol{\chi}_{4\text{-}6} \cdot a_{As1}\left(t_0\right) = 0, \tag{13}$$

$$H\left(t_f\right) - \boldsymbol{\chi}_{7\text{-}9} \cdot \boldsymbol{v}_{As2}\left(t_f\right) - \boldsymbol{\chi}_{10\text{-}12} \cdot \boldsymbol{a}_{As2}\left(t_f\right) = 0, \tag{14}$$

where $\boldsymbol{a}_{As1}(t_0)$ and $\boldsymbol{a}_{As2}(t_f)$ denote the acceleration of Asteroid 1 at time t_0 and Asteroid 2 at time t_f in HECS, respectively.

There are 8 unknowns of the DT rendezvous problem of solar sailing, including 6-D initial costate vectors $\boldsymbol{\lambda}(t_0)$, t_0 and t_f. And there are the same number of equations, which are called shooting functions, including 6-D eq. (11) and stationary conditions (13) and (14). For convenience, in the process of the numerical solution, we express $\boldsymbol{\chi}_{1\sim12}$ with $\boldsymbol{\lambda}_r(t_0)$, $\boldsymbol{\lambda}_v(t_0)$, $\boldsymbol{\lambda}_r(t_f)$ and $\boldsymbol{\lambda}_v(t_f)$ via eq. (12). Therefore, the Lagrange numerical multipliers $\boldsymbol{\chi}_{1\sim12}$ do not appear in the shooting functions.

It is clear that the time and position vary continuously so that $t_m^- = t_m^+ = t_m$ and $\boldsymbol{r}(t_m^-) = \boldsymbol{r}(t_m^+) = \boldsymbol{r}(t_m)$. Using the PMP, the inner transversal conditions are

$$-\boldsymbol{\lambda}_r\left(t_m^-\right)+\boldsymbol{\lambda}_r\left(t_m^+\right)+\frac{\boldsymbol{\chi}_{\mathrm{GA}}^{\mathrm{TBM}}\cdot\partial\boldsymbol{\psi}_{\mathrm{GA}}^{\mathrm{TBM}}}{\partial\boldsymbol{r}\left(t_m^-\right)}+\frac{\kappa_{\mathrm{GA}}^{\mathrm{TBM}}\cdot\partial\sigma_{\mathrm{GA}}^{\mathrm{TBM}}}{\partial\boldsymbol{r}\left(t_m^-\right)}=0,$$

$$-\boldsymbol{\lambda}_v\left(t_m^-\right)+\frac{\boldsymbol{\chi}_{\mathrm{GA}}^{\mathrm{TBM}}\cdot\partial\boldsymbol{\psi}_{\mathrm{GA}}^{\mathrm{TBM}}}{\partial\boldsymbol{v}\left(t_m^-\right)}+\frac{\kappa_{\mathrm{GA}}^{\mathrm{TBM}}\cdot\partial\sigma_{\mathrm{GA}}^{\mathrm{TBM}}}{\partial\boldsymbol{v}\left(t_m^-\right)}=0,$$

$$\boldsymbol{\lambda}_v\left(t_m^+\right)+\frac{\boldsymbol{\chi}_{\mathrm{GA}}^{\mathrm{TBM}}\cdot\partial\boldsymbol{\psi}_{\mathrm{GA}}^{\mathrm{TBM}}}{\partial\boldsymbol{v}\left(t_m^+\right)}+\frac{\kappa_{\mathrm{GA}}^{\mathrm{TBM}}\cdot\partial\sigma_{\mathrm{GA}}^{\mathrm{TBM}}}{\partial\boldsymbol{v}\left(t_m^+\right)}=0.$$

And the inner stationary condition is

$$H\left(t_m^-\right)-H\left(t_m^+\right)+\frac{\boldsymbol{\chi}_{\mathrm{GA}}^{\mathrm{TBM}}\cdot\partial\boldsymbol{\psi}_{\mathrm{GA}}^{\mathrm{TBM}}}{\partial t_m}+\frac{\kappa_{\mathrm{GA}}^{\mathrm{TBM}}\cdot\partial\sigma_{\mathrm{GA}}^{\mathrm{TBM}}}{\partial t_m}=0.$$

Ref. [26] gives the derivatives of the inner constraints (9) and (10), especially the variables $\boldsymbol{v}_\infty^-$, $\boldsymbol{v}_\infty^+$ and r_p, with respect to the basic variables t_m, $\boldsymbol{r}(t_m)$, $\boldsymbol{v}(t_m^-)$ and $\boldsymbol{v}(t_m^+)$. The inner transversal conditions are

$$\boldsymbol{\lambda}_r\left(t_m^+\right)=\boldsymbol{\lambda}_r\left(t_m^-\right)-\boldsymbol{\chi}_{GA1\sim3}^1, \tag{15}$$

$$\boldsymbol{\lambda}_v\left(t_m^-\right)-\boldsymbol{\chi}_{GA4}^1\boldsymbol{u}^-+\frac{1}{r_{\min}}\kappa_{GA}^1\boldsymbol{A}=0, \tag{16}$$

$$\boldsymbol{\lambda}_v\left(t_m^+\right)=\boldsymbol{\chi}_{GA4}^1\boldsymbol{u}^++\frac{1}{r_{\min}}\kappa_{GA}^1\boldsymbol{B} \tag{17}$$

and the inner stationary condition is

$$\begin{aligned}&H\left(t_m^-\right)-H\left(t_m^+\right)-\boldsymbol{\chi}_{GA1\sim3}^1\cdot\boldsymbol{v}_a\left(t_m\right)\\&+\boldsymbol{\chi}_{GA4}^1\left(\boldsymbol{u}^+-\boldsymbol{u}^-\right)\cdot\boldsymbol{a}_a\left(t_m\right)-\frac{1}{r_{\min}}\kappa_{GA}^1C=0,\end{aligned} \tag{18}$$

where

$$\boldsymbol{u}^\pm\triangleq\frac{\boldsymbol{v}_\infty^\pm}{v_\infty^\pm},$$

$$\boldsymbol{a}_a\left(t_m\right)=-\frac{\mu}{r_a^3\left(t_m\right)}\boldsymbol{r}_a\left(t_m\right),$$

$$\begin{cases}\boldsymbol{A}=\dfrac{r_p}{v_\infty^-}\left[\dfrac{1}{4\sin^2\theta/2\left(1-\sin\theta/2\right)}\left(\boldsymbol{u}^+-\cos\theta\boldsymbol{u}^-\right)-\boldsymbol{u}^-\right]\\\boldsymbol{B}=\dfrac{r_p}{v_\infty^+}\left[\dfrac{1}{4\sin^2\theta/2\left(1-\sin\theta/2\right)}\left(\boldsymbol{u}^--\cos\theta\boldsymbol{u}^+\right)-\boldsymbol{u}^+\right]\\C=r_p\left\{-\dfrac{1}{4\sin^2\theta/2\left(1-\sin\theta/2\right)}\left[\dfrac{1}{v_\infty^+}\left(\boldsymbol{u}^--\cos\theta\boldsymbol{u}^+\right)\right.\right.\\\qquad\left.\left.+\dfrac{1}{v_\infty^-}\left(\boldsymbol{u}^+-\cos\theta\boldsymbol{u}^-\right)\right]+\dfrac{\boldsymbol{u}^+}{v_\infty^+}+\dfrac{\boldsymbol{u}^-}{v_\infty^-}\right\}\cdot\boldsymbol{a}_a\left(t_m\right).\end{cases}$$

The rigid condition is derived as:

$$\kappa_{GA}\cdot\sigma_{GA}^{TBM}=0,\kappa_{GA}\geqslant0. \tag{19}$$

For an intermediate GA, there are 9 unknowns, including the 5-D Lagrange numerical multipliers $\boldsymbol{\chi}_{\mathrm{GA1\text{-}4}}^{\mathrm{TBM}}$ and $\kappa_{\mathrm{GA}}^{\mathrm{TBM}}$, the 3-D velocity vector $\boldsymbol{v}(t_m^+)$ just after GA, and the GA date t_m. Additionally, there is an identical number of equations, including the 4-D equality constraints (9), the 1-D rigid condition (19), the 3-D inner transversal conditions (16) and the 1-D inner stationary condition (18). The velocity increment $\Delta\boldsymbol{v}_{GA}$ is caused by GA, rather than the velocity immediately after GA. Eqs. (15) and (17) are not used as parts of the shooting function but are used to update the position and velocity of the costates immediately after GA. The variations of the mass, as well as its costate, and the position vector are not considered for update because they are continuous just before and after GA.

3 Gravity assist in the full ephemeris model

In a practical mission, the GA is a continuous process, as shown in Figure 2. The sailcraft flies mainly under the GA planet's gravity in the sphere of influence of the GA planet for several days. During the flyby process, the states of the sailcraft are continuous. Therefore, the GA in the full ephemeris model has to be considered to satisfy the precision requirement. This section builds a set of equivalent inner constraints that can describe the GA process accurately, to determine the GA effect, which can freely change the states of the sailcraft.

3.1 The mathematical model

In the Heliocentric transfer trajectory, the sailcraft is subject to not only the Sun's gravity but also the planetary gravity. In HERF, the third body gravity perturbative acceleration $\boldsymbol{f}_{Pl}$ is

$$\boldsymbol{f}_{Pl}=-\frac{\mu_{Pl}}{\left\|\boldsymbol{r}-\boldsymbol{r}_{Pl}\right\|^3}\left(\boldsymbol{r}-\boldsymbol{r}_{Pl}\right)-\frac{\mu_{Pl}}{\left\|\boldsymbol{r}_{Pl}\right\|^3}\boldsymbol{r}_{Pl}, \tag{20}$$

where $\boldsymbol{r}_{Pl}$ denotes the position of the planet in HERF. μ_{Pl} denotes the gravitational constant of the planet.

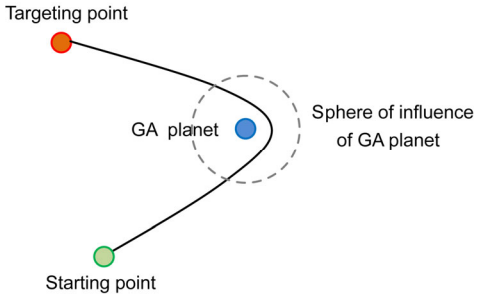

Figure 2 (Color online) Gravity assist process in the full ephemeris model.

The dynamic equation of solar sailing in the full ephemeris model can be written as:

$$\dot{\boldsymbol{r}} = \boldsymbol{v}, \dot{\boldsymbol{v}} = -\frac{\mu}{r^3}\boldsymbol{r} + \sum \boldsymbol{f}_{Pl} + \frac{\beta\mu(\boldsymbol{r}\cdot\boldsymbol{n})^2}{r^4}\boldsymbol{n}, \tag{21}$$

where $\Sigma \boldsymbol{f}_{Pl}$ are all the third-bodies' perturbations, mainly the eight main planets.

The Hamiltonian function $\boldsymbol{H}$ can be expressed as follows:

$$H = \boldsymbol{\lambda}_r \cdot \boldsymbol{v} + \boldsymbol{\lambda}_v \cdot \left(-\frac{\mu}{r^3}\boldsymbol{r} + \sum \boldsymbol{f}_{Pl} + \frac{\beta\mu(\boldsymbol{r}\cdot\boldsymbol{n})^2}{r^4}\boldsymbol{n} \right) - 1. \tag{22}$$

The costate differential functions have changed accordingly and can be derived as:

$$\dot{\boldsymbol{\lambda}}_r = \frac{\mu}{r^3}\boldsymbol{\lambda}_v - \frac{3\mu\boldsymbol{r}\cdot\boldsymbol{\lambda}_v}{r^5}\boldsymbol{r} - \sum \frac{\partial(\boldsymbol{\lambda}_v \cdot \boldsymbol{f}_{Pl})}{\partial \boldsymbol{r}} - 2\beta\mu(\boldsymbol{r}\cdot\boldsymbol{n})(\boldsymbol{\lambda}_v\cdot\boldsymbol{n})\left(\frac{1}{r^4}\boldsymbol{n} - \frac{2(\boldsymbol{r}\cdot\boldsymbol{n})}{r^6}\boldsymbol{r}\right), \dot{\boldsymbol{\lambda}}_v = -\boldsymbol{\lambda}_r, \tag{23}$$

where

$$\frac{\partial(\boldsymbol{\lambda}_v \cdot \boldsymbol{f}_{Pl})}{\partial \boldsymbol{r}} = -\frac{\mu_{Pl}}{\|\boldsymbol{r}-\boldsymbol{r}_{Pl}\|^3}\boldsymbol{\lambda}_v + \frac{3\mu_{Pl}\boldsymbol{\lambda}_v\cdot(\boldsymbol{r}-\boldsymbol{r}_{Pl})}{\|\boldsymbol{r}-\boldsymbol{r}_{Pl}\|^5}(\boldsymbol{r}-\boldsymbol{r}_{Pl}).$$

The optimal normal vector of the solar sail is the same as eqs. (5) and (6), and the differential equation is the same as eq. (7).

3.2 Constraints

3.2.1 Sailcraft launch ($t=t_0$) and Rendezvous ($t=t_f$)

The simplest problem is considered, and the constraints of the sailcraft and rendezvous in the full ephemeris model are the same as the constraints of the sailcraft (8) and rendezvous (11) in the two-body model.

3.2.2 Midcourse flyby($t=t_m$)

The dynamic equation of solar sailing, eq. (20) or (21), in the full ephemeris model has considered all the transfer trajectories both with and without GA, which denotes whether the spacecraft does or does not fly though the sphere of influence of major planet. But when the spacecraft flies through the GA planet's sphere of influence during the flight, the perturbation of the GA planet is obvious, the nonlinearity of the shoot function increases, the domain of convergence becomes narrower, so it is very hard or even impossible to obtain the solution to problem with GA, even if the solution to problem with GA is the global optimal solution. So it is very necessary to add inner constraints to guide the spacecraft to fly though the sphere of influence of major planet to get GA.

The full ephemeris model describes an actural space environment, which can achieve a GA process if the sailcraft flies through the GA planet's sphere of influence. A set of constraints, which correspond to the Lagrange numerical multipliers $\chi_{\mathrm{GA1\text{-}4}}^{\mathrm{FEM}}$, with GA can be built as:

$$\boldsymbol{\psi}_{\mathrm{GA}}^{FEM} \triangleq \begin{pmatrix} \cos\left(i(t_m)\right) - \cos(i_{\mathrm{norm}}) \\ r_{\mathrm{p}}(t_m) - r_{\mathrm{pnorm}} = 0 \\ f(t_m) - f_{\mathrm{norm}} \end{pmatrix} = \boldsymbol{0}, \tag{24}$$

where superscript FEM denotes the quantities in the full ephemeris model, t_m is the time of perigee of the hyperbolic relative to the GA planet. $i(t_m)$, $r_p(t_m)$ and $f(t_m)$are the actual orbit inclination, the perigee distance and the true anomaly of the hyperbolic relative to the GA planet in the full ephemeris model. i_{norm}, r_{pnorm} and f_{norm} are the nominal orbit inclination, the perigee distance and the true anomaly given by the two-body model. The first two equations are to ensure that the sailcraft's states are suitable for the ones given by the two-body model at the perigee time, and the last equation is to ensure that the t_m is the time of perigee of the hyperbolic. Therefore, f_{norm} is set as zero. It is trivial to obtain the true anomaly such that the third equality constraint of (24) is equivalent to

$$\Delta\boldsymbol{r}\cdot\Delta\boldsymbol{v} = \boldsymbol{0}, \tag{25}$$

where Δr and Δv denote the position and velocity of the sailcraft relative to the GA planet in HECS, respectively.

(i) The nominal value of the orbit inclination and the perigee distance. The nominal orbit inclination and the perigee distance can be defined with the incoming and outgoing hyperbolic residual velocity in the two-body model of trajectory with GA. The nominal orbit inclination is defined as:

$$\cos\left(i_{\mathrm{norm}}\right) = h_{\mathrm{norm}z} / \left\|\boldsymbol{h}_{\mathrm{norm}}\right\|, \tag{26}$$

$$\boldsymbol{h}_{\mathrm{norm}} = \frac{\boldsymbol{v}_\infty^- \times \boldsymbol{v}_\infty^+}{\left|\boldsymbol{v}_\infty^- \times \boldsymbol{v}_\infty^+\right|}, h_{\mathrm{norm}z} = \boldsymbol{h}_{\mathrm{norm}}\cdot\boldsymbol{k},$$

where $\boldsymbol{h}_{\mathrm{norm}}$ is the orbital plane normal to the sailcraft relative to the GA planet, and $\boldsymbol{k}$ is the reference unit vector, which is set as the ecliptic plane normal for convenience, $\boldsymbol{k}=(0, 0, 1)^{\mathrm{T}}$.

The nominal perigee distance is defined as:

$$r_{\mathrm{pnorm}} = \frac{\mu_a}{v_\infty^2}\left(\frac{1}{\sin\frac{\theta}{2}} - 1\right), \tag{27}$$

where θ is rotation angle of the hyperbolic excess speed for the planetary GA, which is defined as:

$$\sin\frac{\theta}{2} = \sqrt{\frac{1-\cos\theta}{2}}, \quad \cos\theta = \frac{\boldsymbol{v}_\infty^- \cdot \boldsymbol{v}_\infty^+}{v_\infty^2}.$$

(ii) The actual orbit inclination, the perigee distance and the true anomaly. The actual orbit inclination, the perigee

distance and the true anomaly can be calculated with the actual position and velocity vector relative to the GA planet. The actual orbit inclination is defined as:

$$\cos\left(i(t_m)\right)=h_z/h, \tag{28}$$

where $\boldsymbol{h}$ is the Angular momentum of the sailcraft relative to the GA planet:

$$\boldsymbol{h}=\Delta\boldsymbol{r}(t_m)\times\Delta\boldsymbol{v}(t_m),\quad h_z=\boldsymbol{h}\cdot\boldsymbol{N},$$

where $\Delta\boldsymbol{r}(t_m)$ and $\Delta\boldsymbol{v}(t_m)$ denote the position and velocity with respect to the GA planet.

The actual semimajor axis is

$$a(t_m)=\frac{\mu_{Pl}}{\left(\dfrac{2\mu_{Pl}}{\Delta r(t_m)}-\Delta v^2(t_m)\right)}$$

and the eccentricity vector is

$$\boldsymbol{e}=\frac{1}{\mu_{Pl}}\left[\left(\Delta v(t_{\mathrm{m}})^2-\frac{\mu_{Pl}}{\Delta r(t_{\mathrm{m}})}\right)\Delta\boldsymbol{r}(t_{\mathrm{m}})-\left(\Delta\boldsymbol{r}(t_{\mathrm{m}})\cdot\Delta\boldsymbol{v}(t_{\mathrm{m}})\right)\Delta\boldsymbol{v}(t_{\mathrm{m}})\right],$$

so the perigee distance is defined as:

$$r_p\left(t_m\right)=a(1-e). \tag{29}$$

3.3 Nonlinear equation solver

The boundary transversal conditions and the stationary conditions are the same as eqs. (12)–(14).

According to the PMP, the inner transversal conditions are

$$-\boldsymbol{\lambda}\left(t_m^-\right)+\boldsymbol{\lambda}\left(t_m^+\right)+\frac{\boldsymbol{\chi}_{\mathrm{GA}}^{\mathrm{FEM}}\cdot\partial\boldsymbol{\psi}_{\mathrm{GA}}^{\mathrm{FEM}}}{\partial\boldsymbol{x}\left(t_m\right)}=0, \tag{30}$$

and the inner stationary condition is

$$H\left(t_m^-\right)-H\left(t_m^+\right)+\frac{\boldsymbol{\chi}_{\mathrm{GA}}^{\mathrm{FEM}}\cdot\partial\boldsymbol{\psi}_{\mathrm{GA}}^{\mathrm{FEM}}}{\partial t_m}=0. \tag{31}$$

The derivation of deriving the derivatives of the inner constraints with respect to the basic variables is listed in the appendix.

There are four extra unknowns in all, including the 3-D Lagrange numerical multipliers $\boldsymbol{X}_{\mathrm{GA}}$ and the event time t_m. There are identical numbers of equations, including the 3-D equation (24) and the inner stationary condition (31). It is important to note that transversal condition (30) is not used to constitute the targeting functions but is used to update the value of the costate vectors at the event time t_m. The values of the position vectors and the velocity vectors of the sailcraft are continuous at the event time t_m; therefore, they need not be updated.

4 Numerical simulations

One example of the time optimal problem with a single Earth gravity assist (EGA), both in the two-body model and the full ephemeris model, will be given to substantiate the techniques and theories presented in sect. 2 and 3. The heliocentric position, velocity and orbit elements of the planets are computed online by the JPL Horizons system.

In the numerical results, we multiply the performance index by a positive unknown factor λ_0 to make the optimal control problem homogeneous to the Lagrange multipliers including this factor [26]. Hence, normalization is applicable to restrict the unknown multipliers on a unit hypersphere, which can enhance the possibility of converging to the global optimal solution.

For calculation convenience, the quantities of length and time are normalized by astronomy units (AU, 149597870.66 km), and years (a, 356.25×86400 s), respectively. Therefore, the value of μ should be 39.476926 $\mathrm{AU}^3/\mathrm{a}^2$. The other values should be transformed into those consistent with the normalized units. Because Uranus and Neptune are too far from the solar sail and because the gravitational perturbation to the solar sail is minimal, we only consider the other six main planets, of which the gravitational constant and the minimal admissible periapsis radius are listed in Table 1.

4.1 Examples of a mission using direct transfer (DT) and a mission including a single EGA in the two-body model

4.1.1 A rendezvous problem between two fixed trajectories with fixed β

For the sake of demonstrate the effect of EGA on trip time, the rendezvous problem from Asteroid 1 to Asteroid 2 is considered. This example, which avoids the escaping orbit and capture orbit, is chosen to highlight the core technique in sect. 2. The elements of the Earth, Asteroid 1 and Asteroid 2 are listed in Table 2. The sail lightness number is set as β=0.1.

Table 1 The values of the parameters of the six main planets

Main planets	Mercury	Venus	Earth	Mars	Jupiter	Saturn
Gravitational constants μ_{Pl} ($\mathrm{km}^3/\mathrm{s}^2$)	22032.1	324859.0	398600.0	42828.3	1.26687×10^8	3.79313×10^7
The minimal admissible periapsis radius $r_{\min\ Pl}$ (km)	2740.0	6373.0	6678.0	3689.9	71700.0	60568.0

Table 2 The orbital elements of Asteroid 1, Earth and Asteroid 2

Orbital element	Asteroid 1	The Earth	Asteroid 2
t (MJD)	54000.000	54000.000	54000.000
a (AU)	0.800000	1.000840	1.500000
e	0.016507	0.016507	0.016507
i (°)	0.001218	0.001218	0.001218
Ω (°)	1.770191	1.770191	1.770191
ω (°)	98.504893	98.504893	98.504893
f (°)	240.000000	260.350296	320.000000

The techniques presented in sect. 2 are applied to solve the time-optimal rendezvous problem of DT and EGA. The results are listed in Table 3, which shows that the trip time using EGA (549.308 d) is 127.682 d shorter than the trip time (676.990) using direct transfer.

The transfer trajectory is shown in Figure 3, from which it can be observed that the sailcraft of the mission using EGA starts later from the orbit of Asteroid 1 and targets the orbit of Asteroid 1 earlier than when using DT.

Figure 4 shows the energy-changing curve. From the figure, it can be seen that the energy of the sailcraft is continuous and gradually increases from the energy of the orbit of asteroid 1 to the energy of the orbit Asteroid 2 because of the solar radiation pressure in DT. However, the energy of the sailcraft is discontinuous at the EGA time and increases instantly because of the EGA when using EGA, which shows the effect of EGA intuitively.

4.1.2 A rendezvous problem between two fixed trajectories under different β

For the mission, significant propellant mass saving may be obtained with the use of complex multiple intermediate flyby maneuvers, but the corresponding trip time increase is substantial in many cases. This section discusses the trip time of a mission using DT and a mission using EGA, along with the change of the sail lightness number $\beta\in[0.06,0.15]$. The same rendezvous problem from Asteroid 1 to Asteroid 2 is considered, and the elements of the Earth, Asteroid 1 and Asteroid 2 are listed in Table 2.

Figure 5 shows that the trip time of both the mission using DT and the mission using EGA decreases with the increase of β because the propulsion capability of the sailcraft increases with the increase of β. This result also shows that the smaller the β is, the more obvious is the decrease of trip time when using EGA. However, when $\beta\leqslant0.07$, the trip time increases markedly because it costs the sailcraft a significant length of time to approach Earth to achieve EGA.

4.1.3 A rendezvous problem targets different trajectories with fixed β

This part discusses the trip time of the mission using DT and the mission using EGA along with the change of the semi-major axis of Asteroid 2, where $a_2\in[1.32\text{AU},1.58\text{AU}]$. The elements of the Earth, Asteroid 1 and 2 are listed in Table 4.

Figure 6 shows that the trip time increases with respect to the increas of the difference between the initial orbital energy and the final orbital energy in both the DT and the EGA. It shows that the larger the difference between the

Table 3 The results of the two-body model both with and without EGA

Parameter	Director transfer	Earth gravity assist
The starting time t_0 (MJD)	53907.952	53989.824
The EGA time t_m (MJD)	–	54092.843
The targeting time t_f (MJD)	54584.942	54539.132

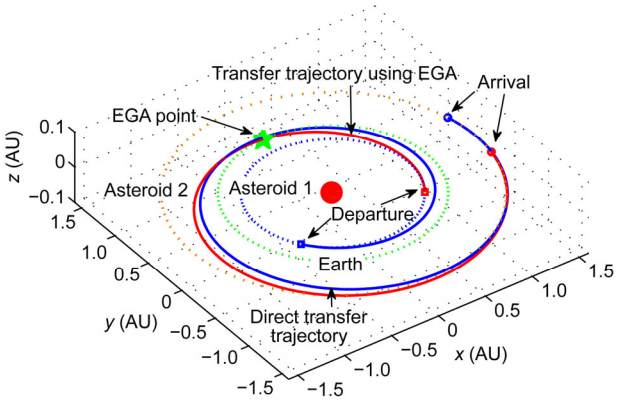

Figure 3 (Color online) The optimal transfer trajectory in a two-body model.

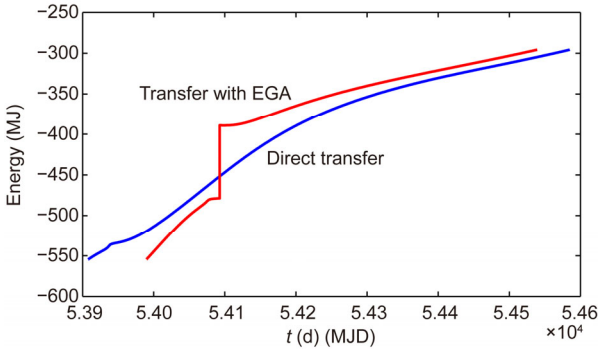

Figure 4 (Color online) Energy-changing curve in the two-body model.

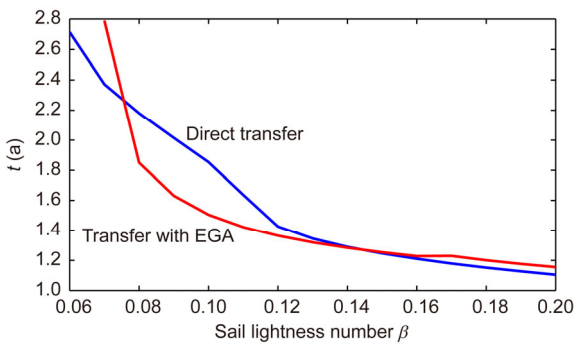

Figure 5 (Color online) The change of trip time relative to β.

Table 4 The orbital elements of Asteroid 1, Earth and Asteroid 2

Orbital element	Asteroid 1	The Earth	Asteroid 2
t (MJD)	54000.000	54000.000	54000.000
a (AU)	0.800000	1.000840	a_2
e	0.016507	0.016507	0.016507
i (°)	0.001218	0.001218	0.001218
Ω (°)	1.770191	1.770191	1.770191
ω (°)	98.504893	98.504893	98.504893
f (°)	240.000000	260.350296	320.000000

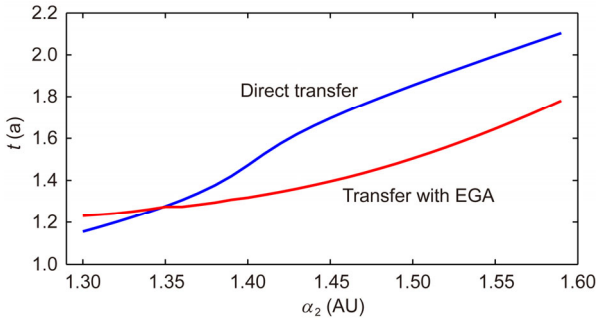

Figure 6 (Color online) The change of trip time relative to a_2.

initial orbital energy and the final orbital energy, the more obvious the decrease of trip time when using EGA compared to DT, which shows that EGA is more useful when the difference between the initial orbital energy and the final orbital energy is large.

4.2 Examples with EGA in the two-body model and the full ephemeris model

The same rendezvous problem from Asteroid 1 to Asteroid 2 is considered. The elements of the Earth, Asteroid 1 and Asteroid 2 are the same as in Table 2.

Table 5 lists the results of the time optimal problem of a solar sail with EGA designed in the two-body model, including the initial time, the final time, the hyperbolic excess velocity $\boldsymbol{v}_\infty^-$ and $\boldsymbol{v}_\infty^+$, the minimal value of the constraints and the related parameters are given via TBM. All the vectors are projected into HECS.

In making the numerical solution more convenient, the time of the perigee of Earth is set as the event time. Because of the highly nonlinear, highly sensitive initial values of the costate vectors in the fuel-optimal problem in the full ephemeris model, the beforehand mission has to be solved, which starts from Asteroid 1 and arrives at the GA planet, Earth. In the beforehand mission, the initial state and the starting time are identical to the primal mission above, and the final boundary value is the same as the inner constraints of the mission. The solution of the two-body model is given to the equation of the beforehand mission, and then the solution of the beforehand mission is given to the primal mission. Table 6 lists the results of the time optimal problem of a solar sail with EGA designed in the full ephemeris model, including the initial time, the final time, and so on. All the vectors are projected into HECS. By comparison between table 5 and table 6 of the starting times, the targeting time of

Table 5 The results obtained via the two-body model

Variables	Value
Starting time (MJD)	53989.824
Event time (MJD)	54092.844
Targeting time (MJD)	54539.131
The incoming hyperbolic exceeding velocity $\boldsymbol{v}_\infty^-$ (km/s)	$[-1.418000,\ 4.718120,\ 9.934324\times10^{-5}]$
The outgoing hyperbolic vxceeding velocity $\boldsymbol{v}_\infty^+$ (km/s)	$[-1.541324,\ 4.679863,\ 1.004324\times10^{-4}]$
The velocity increment $\Delta\boldsymbol{v}_{\rm GA}$ (km/s)	$[-2.959432,\ -3.864432\times10^{-2},\ 1.122234\times10^{-6}]$
Rotation angle δ_0 (°)	1.496
The trip time Δt (d)	549.307
The nominal value designed via TBM $\cos i_{\rm norm}$	0.997
The nominal value designed via TBM $r_{p\rm norm}$ (km/s)	3.824941×10^4

Table 6 The results obtained via the full ephemeris model

Variables	Value
Starting time (MJD)	53990.142
Time of perigee of Earth (MJD)	54092.844
Targeting time (MJD)	54539.132
The time entering the sphere of influence of GA planet (MJD)	54090.838
The exceed velocity when entering the sphere of influence of GA planet (km/s)	$[1.440939, 4.811423, 1.012583\times10^{-4}]$
The time leaving the sphere of influence of GA planet (MJD)	54094.930
The exceed velocity when leaving the sphere of influence of GA planet (km/s)	$[-1.565568, 4.769470, 1.012583\times10^{-4}]$
The velocity increment $\Delta\boldsymbol{v}_{\rm GA}$ (km/s)	[−3.006507, −0.041953, 0.000000]
The fly time through the sphere of influence of GA planet Δt (d)	4.092
The trip time Δt (d)	549.307

the full ephemeris model is close to the time corresponding to the variables in the two-body model. The difference between the two model missions is small, only 5.771×10^{-4} d.

Figure 7 shows the transfer trajectories of the two-body model and the full ephemeris model, and the two curves are almost overlapping with the starting point and targeting point of both models close together. Figure 8 shows that the optimal control rate of the sailcraft in the full ephemeris model is similar to the consumption and similar to the optimal control rate in the two-body model, which shows that the results obtained via the two-body model are reasonable.

Figure 9 shows the changing trend of the main force and the perturbation during the flight in the full ephemeris model. The sun's gravitational acceleration is approximately 5×10^{-6} km/s^2, the solar radiation pressure is approximately 5×10^{-8} km/s^2, and both of them decrease as the sailcraft flies away from the Sun. As the sailcraft gains energy by virtue of EGA, the Earth's gravitational acceleration becomes the main force when the sailcraft flies through the sphere of influence of the Earth, and the magnitude of Earth's gravitational acceleration is approximately 5×10^{-4} km/s^2. The figure shows that the main perturbations are Jupiter's gravitational acceleration and Venus's gravitational acceleration.

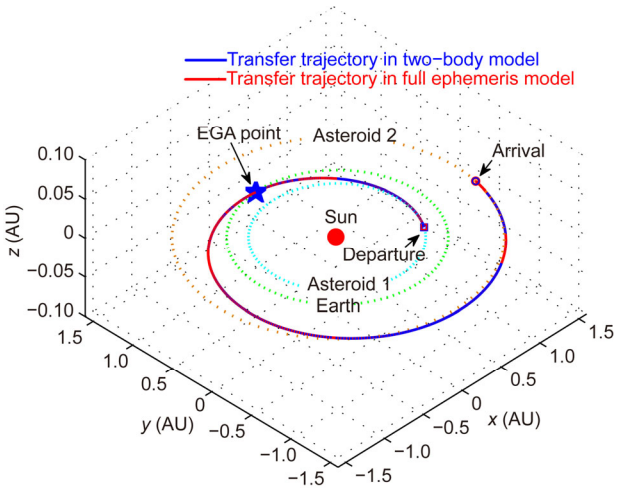

Figure 7 (Color online) The optimal transfer trajectory in the two-body model and the full ephemeris model.

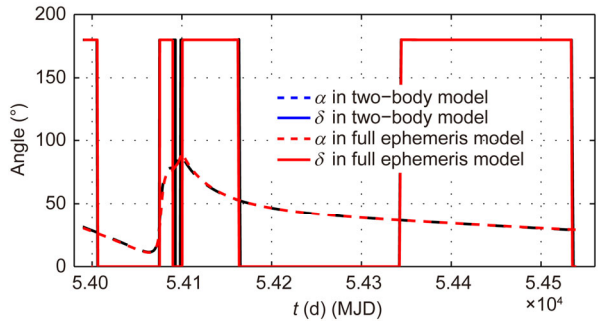

Figure 8 (Color online) The sail altitude control profile.

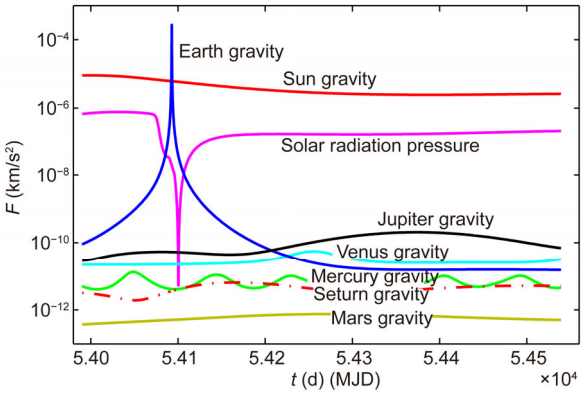

Figure 9 (Color online) The main force and the perturbation in the full ephemeris model.

Figure 10 shows the Energy curve of the sailcraft in both models. The two curves are similar when the sailcraft is far from the Earth. At the event time in the two-body model, the energy curve jumps substantially, which shows that the sailcraft gains substantial energy via EGA. In the full ephemeris model, the curve increases gradually, and the EGA process costs approximately over 4 d, in which the sailcraft flies through the sphere of influence of the GA planet. The figure shows that when the sailcraft flies away from the Earth, the energy curve decreases a little because of the resistance from Earth's gravity.

5 Conclusions

For the sailcraft, whose performance index is the trip time, the employment of the flyby maneuver reduces the total mission energy requirement, but it also increases both the mission complexity and the trip time. When the sail lightness number β is small, the trip time of the direct transfer (DT) is large, and using gravity assist (GA) can reduce the trip time. The decrease is more significant when β is smaller. For the rendezvous problem, when the energy difference of the initial and final orbit is large, the trip time of DT is long, using GA can also decrease the trip time, and the decrease is more significant when the difference is larger. For low performance (β is small) solar sails, multiple flyby maneuvers should be considered to decrease the trip time when the energy difference between the initial and final orbit is large.

Compared to the two-body model, the solar sailing trajectory design in the full ephemeris model is much closer to the real problem. This design introduces the third-body gravity perturbation, especially the GA planet's gravity, and it can describe the GA process more accurately. A set of inner constraints, including the actual orbit inclination, the perigee distance and the true anomaly constraints, can guide the sailcraft flying through the sphere of influence of the GA planet and finishing the GA process. However, because

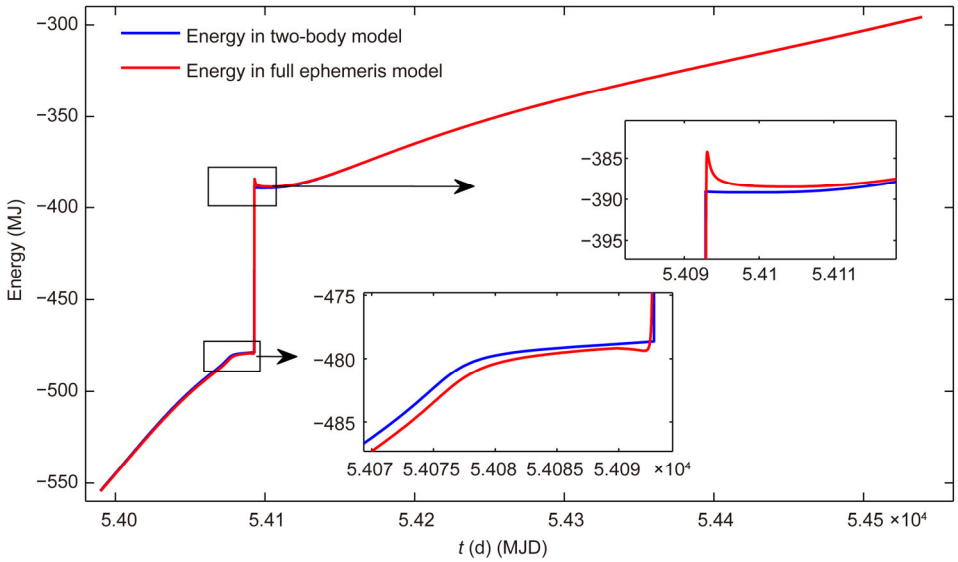

Figure 10 (Color online) Energy-changing curve in the two-body model and the full ephemeris model.

of the strong nonlinearity of the dynamic equations in the sphere of influence of the GA planet, it is more difficult to find the optimal solution in the full ephemeris model than in the two-body mode. The differences of the optimal results, including the trip time, sail altitude control profile and the transfer trajectory, are small between the two-body model and the full ephemeris model, which indicates that the two-body model is quite rational in primary design.

Appendix

The inner constraints are associated with the intermediate state and time. The work left is to derive the derivatives of the inner constraints (24), in other words, $i(t_m)$, $r_p(t_m)$ and $f(t_m)$, with respect to the basic variables $\boldsymbol{r}(t_m)$, $\boldsymbol{v}(t_m)$ and t_m. For convenience, we omit the "(t_m)" after the variables a, $\boldsymbol{e}$, e, i, $\boldsymbol{h}$, h, $\boldsymbol{r}$, r, $\boldsymbol{v}$ and v in the deriving, and all of these variables are the values at t_m.

The Partial derivatives to $\boldsymbol{x}(\boldsymbol{t_m})$ and t_m of the inner constraints are

$$\frac{\partial(\cos i-\cos i_{norm})}{\partial x(t_m)}=-\frac{1}{h^3}\frac{\partial \boldsymbol{h}}{\partial \boldsymbol{x}(t_m)}\cdot\boldsymbol{h}\cdot\boldsymbol{h}^{\mathrm{T}}\cdot\boldsymbol{k}+\frac{1}{h}\frac{\partial \boldsymbol{h}}{\partial \boldsymbol{x}(t_m)}\cdot\boldsymbol{k},$$

where $\boldsymbol{h}$ is the column vector, and $\boldsymbol{h}^{\mathrm{T}}$ is the row vector. If an arbitrary column vector $\boldsymbol{a}=(a_1, a_2, a_3)^{\mathrm{T}}$, we denote $\hat{\boldsymbol{a}}$ as:

$$\hat{\boldsymbol{a}}=\begin{bmatrix}\boldsymbol{0} & -a_3 & a_2\\ a_3 & 0 & -a_1\\ -a_2 & a_1 & 0\end{bmatrix}$$

and $\hat{\boldsymbol{a}}^{\mathrm{T}}=-\hat{\boldsymbol{a}}$. Thus,

$$\frac{\partial \boldsymbol{h}}{\partial \boldsymbol{x}(t_m)}=\frac{\partial\left(\Delta\boldsymbol{r}\times\Delta\boldsymbol{v}\right)}{\partial \boldsymbol{x}(t_m)}=\frac{\partial\Delta\boldsymbol{r}}{\partial \boldsymbol{x}(t_m)}\cdot\Delta\hat{\boldsymbol{v}}-\frac{\partial\Delta\boldsymbol{v}}{\partial \boldsymbol{x}(t_m)}\Delta\hat{\boldsymbol{r}}$$

and the partial derivative to the t_m of the cosine of the orbit inclination is

$$\frac{\partial(\cos i-\cos i_{norm})}{\partial t_m}=-\frac{1}{h^3}\left(\frac{\partial \boldsymbol{h}}{\partial t_m}\cdot\boldsymbol{h}\right)\cdot\boldsymbol{h}(t_m)\cdot\boldsymbol{k}+\frac{1}{h}\frac{\partial \boldsymbol{h}}{\partial t_m}\cdot\boldsymbol{k},$$

where

$$\frac{\partial \boldsymbol{h}}{\partial t_m}=\frac{\partial\Delta\boldsymbol{r}}{\partial t_m}\times\Delta\boldsymbol{v}+\Delta\boldsymbol{r}\times\frac{\partial\Delta\boldsymbol{v}}{\partial t_m},$$

$$\frac{\partial\Delta\boldsymbol{r}(t_m)}{\partial t_m}=-\boldsymbol{v}_{Pl}(t_m),\frac{\partial\Delta\boldsymbol{v}(t_m)}{\partial t_m}=-\boldsymbol{a}_{Pl}(t_m).$$

The partial derivative to $\boldsymbol{x}(t_m)$ of the perigee distance is

$$\frac{\partial\left(r_p-r_{pnorm}\right)}{\partial \boldsymbol{x}(t_m)}=(1-e)\frac{\partial a}{\partial \boldsymbol{x}(t_m)}-a\frac{\partial e}{\partial \boldsymbol{x}(t_m)},$$

where

$$\frac{\partial a}{\partial \boldsymbol{x}(t_m)}=\frac{2\mu_{Pl}}{\left(\dfrac{2\mu_{Pl}}{\Delta r}-\Delta v^2\right)^2}\left(\frac{\mu_{Pl}}{\Delta r^2}\frac{\partial\Delta r}{\partial \boldsymbol{x}(t_m)}+\Delta v\frac{\partial\Delta v}{\partial \boldsymbol{x}(t_m)}\right),$$

$$\frac{\partial e}{\partial \boldsymbol{x}(t_m)}=\frac{1}{e}\frac{\partial \boldsymbol{e}}{\partial \boldsymbol{x}(t_m)}\cdot\boldsymbol{e},$$

where

$$\frac{\partial\Delta r}{\partial \boldsymbol{x}(t_m)}=\frac{1}{\Delta r}\frac{\partial\Delta\boldsymbol{r}}{\partial \boldsymbol{x}(t_m)}\cdot\Delta\boldsymbol{r},$$

$$\frac{\partial\Delta v}{\partial \boldsymbol{x}(t_m)}=\frac{1}{\Delta v}\frac{\partial\Delta\boldsymbol{v}}{\partial \boldsymbol{x}(t_m)}\cdot\Delta\boldsymbol{v},$$

$$\frac{\partial \boldsymbol{e}}{\partial \boldsymbol{x}(t_m)}=\frac{1}{\mu_{Pl}}\left(2\Delta v\frac{\partial \Delta v}{\partial \boldsymbol{x}(t_m)}+\frac{\mu_{Pl}}{\Delta r^2}\frac{\partial \Delta r}{\partial \boldsymbol{x}(t_m)}\right)\Delta \boldsymbol{r}^{\mathrm{T}}+\frac{1}{\mu_{Pl}}\left(\Delta v^2-\frac{\mu_{Pl}}{\Delta r}\right)\frac{\partial \Delta \boldsymbol{r}}{\partial \boldsymbol{x}(t_m)}-\frac{1}{\mu_{Pl}}\left(\frac{\partial \Delta \boldsymbol{r}}{\partial \boldsymbol{x}(t_m)}\cdot\Delta \boldsymbol{v}\right)\Delta \boldsymbol{v}^{\mathrm{T}}-\frac{1}{\mu_{Pl}}\left(\frac{\partial \Delta \boldsymbol{v}}{\partial \boldsymbol{x}(t_m)}\cdot\Delta \boldsymbol{r}\right)\Delta \boldsymbol{v}^{\mathrm{T}}-\frac{1}{\mu_{Pl}}\left(\Delta \boldsymbol{r}\cdot\Delta \boldsymbol{v}\right)\frac{\partial \Delta \boldsymbol{v}}{\partial \boldsymbol{x}(t_m)}.$$

The partial derivative to t_m of the perigee distance is

$$\frac{\partial (r_p-r_{pnorm})}{\partial t_m}=(1-e)\frac{\partial a}{\partial t_m}-a\frac{\partial e}{\partial t_m},$$

where

$$\frac{\partial a}{\partial t_m}=\frac{2\mu_{Pl}}{\left(\frac{2\mu_{Pl}}{\Delta r}-\Delta v^2\right)^2}\left(\frac{\mu_{Pl}}{\Delta r^2}\frac{\partial \Delta r}{\partial t_m}+\Delta v\frac{\partial \Delta v}{\partial t_m}\right),$$

$$\frac{\partial e}{\partial t_m}=\frac{1}{e}\frac{\partial \boldsymbol{e}}{\partial t_m}\cdot\boldsymbol{e},$$

where

$$\frac{\partial \Delta r}{\partial t_m}=\frac{1}{\Delta r}\frac{\partial \Delta \boldsymbol{r}}{\partial t_m}\cdot\Delta \boldsymbol{r},\quad \frac{\partial \Delta v}{\partial t_m}=\frac{1}{\Delta v}\frac{\partial \Delta \boldsymbol{v}}{\partial t_m}\cdot\Delta \boldsymbol{v},$$

$$\frac{\partial \boldsymbol{e}}{\partial t_m}=\frac{1}{\mu_{Pl}}\left(2\Delta v\frac{\partial \Delta v}{\partial t_m}+\frac{\mu_{Pl}}{\Delta r^2}\frac{\partial \Delta r}{\partial t_m}\right)\Delta \boldsymbol{r}+\frac{1}{\mu_{Pl}}\left(\Delta v^2-\frac{\mu_{Pl}}{\Delta r}\right)\frac{\partial \Delta \boldsymbol{r}}{\partial t_m}-\frac{1}{\mu_{Pl}}\left(\frac{\partial \Delta \boldsymbol{r}}{\partial t_m}\cdot\Delta \boldsymbol{v}\right)\Delta \boldsymbol{v}-\frac{1}{\mu_{Pl}}\left(\frac{\partial \Delta \boldsymbol{v}}{\partial t_m}\cdot\Delta \boldsymbol{r}\right)\Delta \boldsymbol{v}-\frac{1}{\mu_{Pl}}\left(\Delta \boldsymbol{r}\cdot\Delta \boldsymbol{v}\right)\frac{\partial \Delta \boldsymbol{v}}{\partial t_m}.$$

The partial derivative to $\boldsymbol{x}(t_m)$ of the third is

$$\frac{\partial (\Delta \boldsymbol{r}\cdot\Delta \boldsymbol{v})}{\partial \boldsymbol{x}(t_m)}=\frac{\partial \Delta \boldsymbol{r}}{\partial \boldsymbol{x}(t_m)}\cdot\Delta \boldsymbol{v}+\frac{\partial \Delta \boldsymbol{v}}{\partial \boldsymbol{x}(t_m)}\cdot\Delta \boldsymbol{r}.$$

1 Friedman L. Star Sailing: Solar Sailing and Interstellar Travel. New York: The Wiley Science Publications, 1988
2 Vulpetti G. Solar Sails: A Novel Approach to Interplanetary Travel. New York: The Praxis Publishing, Ltd, 2008
3 Leipold M, Fichtner H, Heber B, et al. Heliopause explorer—a sailcraft mission to the outer boundaries of the solar system. Acta Astronaut, 2006, 59(8-11): 785–796
4 Sweetser T, Peterson C, Nilsen E, et al. Venus sample return missions-a range of science, a range of costs. Acta Astronaut, 2003, 52(2): 165–172
5 Mori O, Tsuda Y, Sawada H, et al. Deployment and steering dynamics of spinning solar sail "IKAROS". In: Second International Symposium on Solar Sailing. New York: Brooklyn, 2010
6 Dachwald B. Optimization of interplanetary solar sailcraft trajectories using evolutionary neurocontrol. J Guidance Control Dyn, 2004, 27(1): 66–72
7 Hughes G, Macdonald M, McInnes C. Sample return from Mercury and other terrestrial planets using solar sail propulsion. J Spacecraft Rocket, 2006, 43(4): 828–835
8 Polites M, Kalmanson J, Mangus D. Solar sail attitude control using small reaction wheels and magnetic torquers. J Aerospace Eng, 2008, 222(1): 53–62
9 Gong S P, Li J F, BaoYin H X. Passive stability design for the solar sail on displaced orbits. J Spacecraft Rocket, 2007, 44(5): 1071–1080
10 Gong S P, Li J F, Baoyin H X. Analysis of displaced solar sail orbits with passive control. J Guidance Control Dyn, 2008, 31(3): 782–785
11 Gong S P, Li J F, Zhu K J. Dynamical analysis of a spinning solar sail. Adv Space Res, 2011, 48(11): 1797–1809
12 MacDonald M, McInnes C, Dachwald B. Heliocentric solar sail orbit transfers with locally optimal control laws. J Spacecraft Rocket, 2007, 44(1): 273–276
13 Gong S P, Li J F. Fuel consumption for interplanetary missions of solar sailing. Sci China-Phys Mech Astron, 2014, 57(3): 521–531
14 Gong S P, Li J F, Gao Y F. Solar sail time-optimal interplanetary transfer trajectory design. Res Astron Astrophys, 2011, 11(8): 981–996
15 McInnes C. Solar sailing: Orbital mechanics and mission applications. Adv Space Res, 2003, 31(8): 1971–1980
16 McAdams J, Dunham D, Farquhar R, et al. Trajectory design and maneuver strategy for the messenger mission to Mercury. J Spacecraft Rockets, 2006, 43(5): 1054–1064
17 Quarta A, Mengali G. Solar sail missions to Mercury with Venus gravity assist. Acta Astronaut, 2009, 65(3-4): 495–506
18 Broucke R. The celestial mechanics of gravity assist. In: AIAA/AAS Astrodynamics Conference, Minneapoils, MN, 15–18 Aug, 1988
19 Prado A. Powered swingby. J Guidance Control Dyn, 1996, 19(5): 1142–1147
20 Felipe G, Prado A. Classification of out-of-plane swing-by trajectories. J Guidance Control Dyn, 1999, 22(5): 643–649
21 Felipe G, Prado A. Trajectory selection for a spacecraft performing a two-dimensional swing-by. Adv Space Res, 2004, 34(11): 2256–2261
22 Bayliss S. Precision targeting for multiple swingby interplanetary trajectories. J Spacecraft Rockets, 1971, 8(9): 927–931
23 Cai X, Chen Y, Li J. Low-thrust trajectory optimization in a full ephemeris model. Acta Mech Sin, doi: 10.1007/s10409-014-0038-5
24 Kechichian J. Optimal low Earth orbit geostationary Earth orbit intermediate acceleration orbit transfer. J Guidance Control Dyn, 1997, 20(4): 803–811
25 Ranieri C, Ocampo C. Indirect optimization of three-dimensional finite-burning interplanetary transfers including spiral dynamics. J Guidance Control Dyn, 2009, 32(2): 444–454
26 Jiang F, Baoyin H, Li J. Practical techniques for low-thrust trajectory optimization with homotopic approach. J Guidance Control Dyn, 2012, 35(1): 245–258